Shear stress activates mitochondrial oxidative phosphorylation by reducing plasma membrane cholesterol in vascular endothelial cells

Kimiko Yamamoto[a,1], Yoshitsugu Nogimori[a,b], Hiromi Imamura[c], and Joji Ando[d,1]

[a]Laboratory of System Physiology, Department of Biomedical Engineering, Graduate School of Medicine, The University of Tokyo, 113-0033 Tokyo, Japan; [b]Pediatrics, Reproductive, Developmental and Aging Sciences, Graduate School of Medicine, The University of Tokyo, 113-8655 Tokyo, Japan; [c]Laboratory of Functional Biology, Graduate School of Biostudies, Kyoto University, 606-8501 Kyoto, Japan; and [d]Laboratory of Biomedical Engineering, School of Medicine, Dokkyo Medical University, 321-0293 Tochigi, Japan

Vascular endothelial cells (ECs) sense and respond to hemodynamic shear stress, which is critical for circulatory homeostasis and the pathophysiology of vascular diseases. The mechanisms of shear stress mechanotransduction, however, remain elusive. We previously demonstrated a direct role of mitochondria in the purinergic signaling of shear stress: shear stress increases mitochondrial adenosine triphosphate (ATP) production, triggering ATP release and Ca^{2+} signaling via EC purinoceptors. Here, we showed that shear stress rapidly decreases cholesterol in the plasma membrane, thereby activating mitochondrial ATP production. Imaging using domain 4 mutant-derived cholesterol biosensors showed that the application of shear stress to cultured ECs markedly decreased cholesterol levels in both the outer and inner plasma membrane bilayers. Flow cytometry showed that the cholesterol levels in the outer bilayer decreased rapidly after the onset of shear stress, reached a minimum (around 60% of the control level) at 10 min, and plateaued thereafter. After the shear stress ceased, the decreased cholesterol levels returned to those seen in the control. A biochemical analysis showed that shear stress caused both the efflux and the internalization of plasma membrane cholesterol. ATP biosensor imaging demonstrated that shear stress significantly increased mitochondrial ATP production. Similarly, the treatment of cells with methyl-β-cyclodextrin (MβCD), a membrane cholesterol-depleting agent, increased mitochondrial ATP production. The addition of cholesterol to cells inhibited the increasing effects of both shear stress and MβCD on mitochondrial ATP production in a dose-dependent manner. These findings indicate that plasma membrane cholesterol dynamics are closely coupled to mitochondrial oxidative phosphorylation in ECs.

endothelial cells | shear stress | cholesterol | mitochondria | ATP

Vascular endothelial cells (ECs) recognize shear stress, a biomechanical force generated by flowing blood, and transduce it into intracellular biochemical signals, thereby causing responses such as changes in cell morphology, function, and gene expression (1). These EC responses play crucial roles in maintaining the homeostasis of the circulatory system, and their impairments cause various vascular diseases such as hypertension, aneurysm, and atherosclerosis (2–4). To date, numerous studies have elucidated the mechanism of EC mechanotransduction and have revealed a unique feature: shear stress activates multiple signal transduction pathways through a variety of membrane molecules, including ion channels, receptors, and adhesion proteins, almost simultaneously (5). Recently, it has become apparent that the plasma membrane itself plays an important role in EC mechanotransduction. EC plasma membranes rapidly respond to shear stress by altering their physical properties, such as fluidity, viscosity, and lipid order (6, 7). We previously demonstrated that shear stress decreases the lipid order of not only EC plasma membranes but also, artificial lipid bilayer membranes, thereby causing a transition from the liquid-ordered state to the liquid-disordered state, along with an increase in membrane fluidity (8). These changes in membrane physical properties were linked to downstream signaling pathways, such as the activation of mitogen-activated protein kinase (9) and the phosphorylation of vascular endothelial growth factor receptors (VEGFRs) (10). This mechanism, in which changes in membrane physical properties occur initially and are then followed by the activation of membrane molecules, may characterize the EC mechanotransduction described above (11).

Ca^{2+} signaling is known to play a critical role in EC mechanotransduction (12). ECs rapidly release intrinsic adenosine triphosphate (ATP) in response to shear stress (13, 14), and this ATP activates purinoceptors, such as ligand-gated channel P2X and G protein-coupled P2Y receptors, located in the plasma membranes; these purinoceptors are responsible for extracellular Ca^{2+} influx and Ca^{2+} release from the endoplasmic reticulum (15–17). The increase in cytoplasmic Ca^{2+} activates a variety of EC functions. In *P2X4*-knockout mice, ECs exhibited neither Ca^{2+} signaling nor the production of a potent vasodilator, nitric oxide, in response to shear stress, thereby impairing the blood flow-dependent vasodilator response and vascular remodeling and resulting in hypertension (4). Our recent study revealed that

---

Significance

The mechanotransduction of shear stress in vascular endothelial cells is still not completely understood. We show a pathway of shear stress signal transduction mediated by plasma membrane cholesterol-dependent mitochondrial oxidative phosphorylation. The latest imaging technology using domain 4 mutant-derived cholesterol biosensors and a fluorescence resonance energy transfer-based adenosine triphosphate (ATP) biosensor revealed that shear stress rapidly decreases cholesterol levels in the plasma membrane via both efflux and internalization, and reduction in plasma membrane cholesterol was linked to the activation of mitochondrial ATP production. The addition of cholesterol blocked these shear stress effects. Increased mitochondrial ATP production led to ATP release from the endothelial cells, thereby activating purinoceptors in the plasma membrane and leading to purinergic Ca^{2+} signaling in response to shear stress.

mitochondria play an important role in shear stress-induced ATP release and Ca^{2+} signaling in ECs (18). Upon shear stress stimulation, the ECs rapidly augmented their mitochondrial ATP production, triggering ATP release and subsequent Ca^{2+} signaling. However, the means by which shear stress acting on the plasma membrane affects mitochondrial oxidative phosphorylation in ECs remains unknown.

Cholesterol plays a dominant role in determining the mechanical properties of plasma membranes by affecting the membrane lipid order, fluidity, bending modulus, thickness, stiffness, and bilayer pressure profile; in this manner, cholesterol modulates the conformation and function of membrane proteins (19). Plasma membrane cholesterol is involved in not only the control of various cell functions, such as signaling, adhesion, motility, and remodeling of the cytoskeleton (20), but also EC responses to biomechanical forces (10, 21–23). For instance, the depletion of EC plasma membrane cholesterol inhibits the shear stress-induced activation of extracellular signal-regulated kinase (22), whereas the addition of cholesterol to EC plasma membranes suppresses the shear stress-induced phosphorylation of VEGFRs (10). However, the roles of plasma membrane cholesterol in EC mechanotransduction have not been fully elucidated, partly because of a lack of information concerning how plasma membrane cholesterol behaves in ECs under shear stress.

In the last decade, domain 4 (D4) of perfringolysin O (PFO), a cholesterol-binding toxin, has been widely used as a cholesterol-specific molecular sensor for measuring and imaging cholesterol in cellular membranes (24). When D4 and its mutants labeled with fluorophores are added to the extracellular medium, cholesterol in the outer leaflet of the plasma membrane can be visualized in living cells; when these sensors are introduced into the cells by gene transfer or microinjection, cholesterol in the inner leaflets of the membrane can be visualized. A recent study showed that these D4-based cholesterol sensors did not lyse the cells or cross the plasma membrane, allowing trans-bilayer asymmetries in plasma membrane cholesterol to be identified in various mammalian cells (25).

In the present study, we applied controlled levels of shear stress to cultured human pulmonary aortic endothelial cells (HPAECs) and examined changes in the amounts and distribution of plasma membrane cholesterol using fluorescence imaging and flow cytometry with D4 mutant-based cholesterol biosensors. We also used biochemical measurements to analyze changes in the amounts of cholesterol in whole cells and isolated plasma membranes. Furthermore, to determine whether changes in plasma membrane cholesterol affect mitochondrial oxidative phosphorylation, we examined changes in mitochondrial ATP concentrations using real-time imaging with a fluorescence resonance energy transfer (FRET)-based ATP biosensor (26).

Results

Visualization of Plasma Membrane Cholesterol in Living Cells Using Recombinant D4 Probes.
HPAECs that had been incubated at room temperature for 10 min in a medium containing EGFP-D4$_{YDA}$ protein or infected with the mCherry-D4$_{YDA}$ adenovirus 2 d earlier were observed using confocal fluorescence microscopy. Confocal images showed that EGFP-D4$_{YDA}$ was distributed along the cell margin, and its distribution was in strong agreement with that of phospholipase C (PLC)-iRFP, a marker protein of the plasma membrane. EGFP-D4$_{YDA}$ did not cross the plasma membrane (*SI Appendix*, Fig. S1). These results indicated that EGFP-D4$_{YDA}$ can depict cholesterol localized to the outer bilayer of the plasma membrane (Fig. 1 *A*, *Top*). Meanwhile, mCherry-D4$_{YDA}$ was distributed along the cell margin, and its distribution was consistent with that of PLC, indicating that mCherry-D4$_{YDA}$ can depict cholesterol localized to the inner bilayer of the plasma membrane (Fig. 1 *A*, *Middle*). mCherry-D4$_{YDA}$ was also distributed in intracellular membranes, with patchy accumulation especially notable around the nucleus. The perinuclear mCherry-D4$_{YDA}$–rich regions were consistent with the presence of GFP-transferrin receptor (TfR), a recycling endosome marker. These findings indicate that cholesterol is abundant not only in the plasma membrane but also, in recycling endosomes (Fig. 1 *A*, *Bottom*).

The treatment of cells with methyl-β-cyclodextrin (MβCD), a membrane-impermeable cholesterol-binding agent that removes membrane cholesterol from the plasma membranes, markedly attenuated both the EGFP-D4$_{YDA}$ and mCherry-D4$_{YDA}$ signals in the plasma membrane (Fig. 1B). When cholesterol was added to the cells, the signals of these two probes at the plasma membrane markedly increased. Quantitative analysis showed that the average fluorescence intensity specific to each probe in both the outer and inner plasma membrane bilayers was significantly reduced by MβCD, while it was clearly increased by the addition of cholesterol (Fig. 1 *C* and *D*). These findings indicate that the localizations of EGFP-D4$_{YDA}$ and mCherry-D4$_{YDA}$ were cholesterol dependent.

Shear Stress Resulted in a Rapid Decrease of Plasma Membrane Cholesterol.
When HPAECs were subjected to a shear stress of 15 dynes/cm^2 for 15 min in a flow-loading apparatus, both the EGFP-D4$_{YDA}$ and mCherry-D4$_{YDA}$ signals localized to the plasma membrane decreased significantly (Fig. 2A). A quantitative analysis showed that shear stress markedly decreased the fluorescence intensities of both probes in the plasma membrane. These findings indicate that shear stress decreased the amount of cholesterol localized to both the outer and inner plasma membrane bilayers.

The decreased cholesterol levels seen in the mCherry-D4$_{YDA}$ image had returned to the control levels when the levels were examined 5 min after the cessation of the shear stress (Fig. 2B). Real-time imaging of mCherry-D4$_{YDA}$ showed that the inner plasma membrane cholesterol level began to decrease immediately after the initiation of shear stress and that the decreased cholesterol levels recovered gradually after the shear stress was stopped (Fig. 2C). These findings indicate that the membrane cholesterol responses were rapid and reversible.

HPAECs labeled with EGFP-D4$_{YDA}$ were subjected to flow cytometry to quantify the cholesterol content of their plasma membrane outer bilayer (Fig. 2D). The cholesterol levels decreased rapidly after the onset of shear stress, reached a minimum value (around 60% of the value for a static control) at 10 min, and plateaued thereafter. After the shear stress ceased, the decreased cholesterol levels returned to the control levels.

When ECs were exposed to shear stresses at different intensities, the cholesterol levels decreased in a dose-dependent manner in the range of 0 to 10 dynes/cm^2; after reaching a minimum at 10 dynes/cm^2, they maintained the same level at 15 dynes/cm^2 (Fig. 2E). Treatment of the cells with MβCD, a cholesterol-depleting agent, reduced the plasma membrane cholesterol levels to less than half of that seen in the control (Fig. 2E).

In flow-loading experiments, ECs were subjected not only to shear stress but also, to pressure that exerted a compressive force on the cell membrane. To determine whether the pressure affected the membrane cholesterol levels, ECs were subjected to a hydrostatic pressure (40 mm Hg) under no-flow conditions. The hydrostatic pressure alone had no effect on the membrane cholesterol levels (Fig. 2E). This means that the flow-induced decrease in plasma membrane cholesterol was attributable to shear stress and not to pressure.

To examine whether other EC lines as well as HPAECs respond to shear stress and reduce plasma membrane cholesterol, shear stress was applied to cultured human aortic endothelial cells (HAECs), human coronary artery ECs, and human umbilical vein ECs, and the changes in plasma membrane cholesterol were measured using flow cytometry. Shear stress significantly decreased the outer bilayer cholesterol levels not only in HPAECs but also, in all of the above EC lines (*SI Appendix*, Fig. S2A).
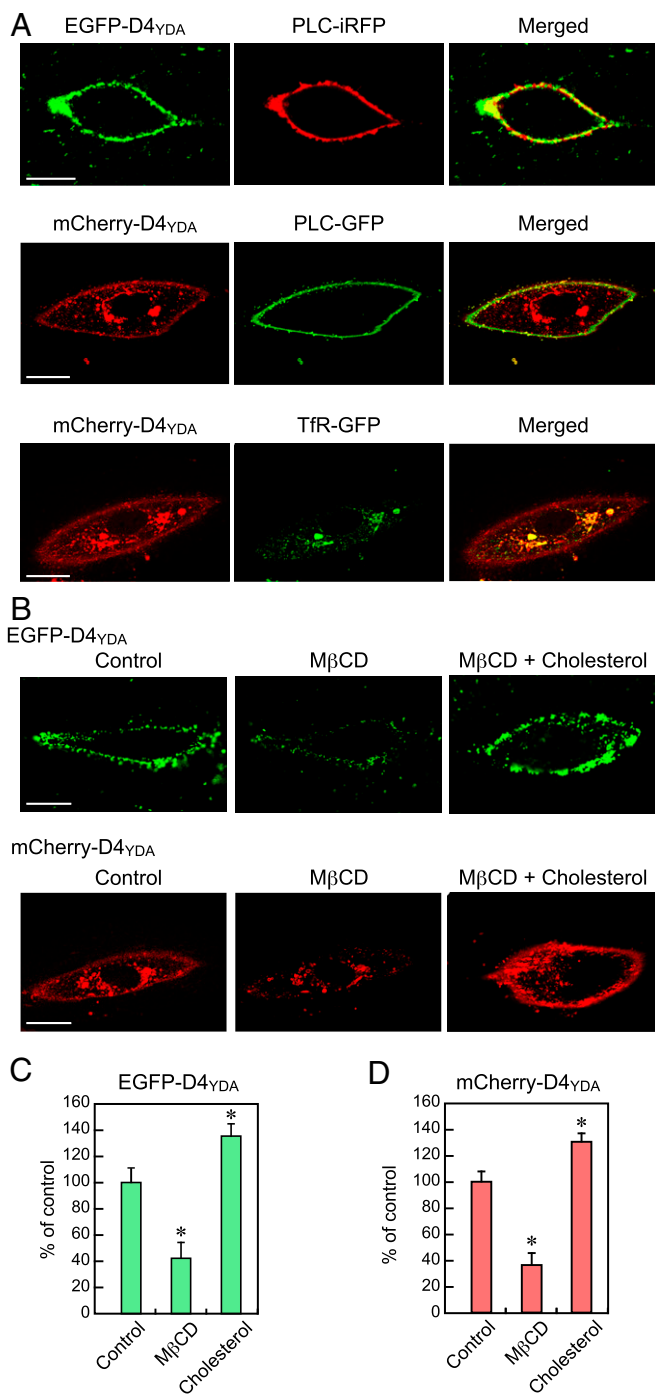
Fig. 1. Visualization of cellular cholesterol using D4 mutant-based cholesterol biosensors. (A) Confocal images of living HPAECs labeled with EGFP-D4$_{YDA}$ and expressing mCherry-D4$_{YDA}$, PLC (PLC-iRFP, PLC-GFP), and TfR (TfR-GFP). EGFP-D4$_{YDA}$ localized to the plasma membranes was visualized using PLC-iRFP, a plasma membrane marker. Expressed mCherry-D4$_{YDA}$ localized to the plasma membrane was visualized using PLC-GFP and was also observed in the perinuclear region. The patchy accumulation of mCherry-D4$_{YDA}$ around the nucleus was colocalized with TfR-GFP, a recycling endosome marker. (Scale bars: 20 μm.) (B) Confocal images of MβCD/cholesterol-treated HPAECs labeled with EGFP-D4$_{YDA}$ and expressing mCherry-D4$_{YDA}$. Treatment of the cells with MβCD (10 mM) for 3 min almost eliminated the EGFP-D4$_{YDA}$ and mCherry-D4$_{YDA}$ signals in the plasma membranes, and the addition of cholesterol (10 mM MβCD plus 50 μM cholesterol) prevented the effects of MβCD and enhanced both probe signals in the plasma membranes, indicating that the localization of both probes was cholesterol dependent. (Scale bars: 20 μm.) (C and D) Quantitative analysis of changes in the plasma

Shear Stress Decreased Both Free and Esterified Cholesterol Mainly in the Apical Plasma Membranes. The apical and basal plasma membranes were separately obtained from HPAECs, and the amount of cholesterol in each membrane was biochemically measured. The application of a shear stress of 15 dynes/cm^2 for 15 min caused a significant decrease in the cholesterol content of the apical plasma membranes, but not in the basal plasma membranes (Fig. 3A). This indicates that the decrease in plasma membrane cholesterol occurred mainly in the apical membrane.

Plasma membranes contain not only free cholesterol but also, esterified cholesterol. The amounts of free and esterified cholesterol were quantified in a biochemical analysis of ECs treated with or without esterase. In the plasma membrane, the amount of esterified cholesterol was around one-fourth that of free cholesterol. Upon shear stress stimulation, the esterified cholesterol as well as the free cholesterol markedly decreased in the apical plasma membranes (Fig. 3A).

Shear Stress Caused Both the Efflux and the Internalization of Plasma Membrane Cholesterol. To examine the destinations of cholesterol leaving the plasma membrane in response to shear stress, the amounts of free cholesterol in both whole cells and isolated plasma membranes were biochemically measured using HPAECs cultured under static conditions or subjected to a shear stress of 15 dynes/cm^2. Upon shear stress stimulation for 15 min, the free cholesterol level in the whole cells decreased to around 80% of the value observed in the control (12.99 ± 1.45 vs. 10.32 ± 0.57 nmol/10^6 cells), while that in the isolated plasma membranes decreased to around 64% of that observed in the control (8.24 ± 0.84 vs. 5.30 ± 1.78 nmol/10^6 cells) (Fig. 3B). The decreased amount of free cholesterol in the plasma membrane was slightly larger than that in the whole cells. Similar shear stress-mediated cholesterol efflux and internalization occurred in HAECs (*SI Appendix*, Fig. S2B). These findings suggest that the majority of cholesterol leaving the plasma membrane moves out of the cell, while the remainder moves into the cell. However, it was not possible to determine the percentage of plasma membrane cholesterol moving out of the cells and that moving into the cells since it was unclear how much intracellular cholesterol in addition to plasma membrane cholesterol moved out of the cell in response to the shear stress. In addition, since plasma membranes are difficult to isolate at high yields, the plasma membranes isolated in the present experiments were expected to be less than the entire plasma membranes.

Decreased Plasma Membrane Cholesterol Is Closely Coupled to the Activation of Mitochondrial Oxidative Phosphorylation. To monitor the changes in mitochondrial ATP levels, we used the genetically encoded FRET-based ATP Biosensor mitAT1.03, which targets the mitochondrial matrix. HPAECs loaded with mitAT1.03 were subjected to a shear stress of 15 dynes/cm^2, and changes in the mitochondrial ATP levels were examined. Pseudocolor images of the yellow fluorescent protein (YFP)-to-cyan fluorescent protein (CFP) ratio showed that the ATP levels markedly increased over the entire mitochondria when cells were subjected to shear stress (Fig. 4A). Changes in the ratio over time were quantified by defining regions of interest in the mitochondria. The ratio rapidly increased after the initiation of shear stress, remained at the increased level, and then returned to the control level after the shear stress ceased. Since the YFP-to-CFP ratio was strongly correlated with the ATP concentrations in mitochondria, these

membrane cholesterol. The fluorescence intensity of each D4-based sensor was measured by setting a region of interest over the plasma membrane. The bar graph shows the changes relative to the control (100%). The data are expressed as the mean ± SD (*n* = 30). All of the above experiments were performed with the cells in a nonconfluent state. *P < 0.01 vs. control.
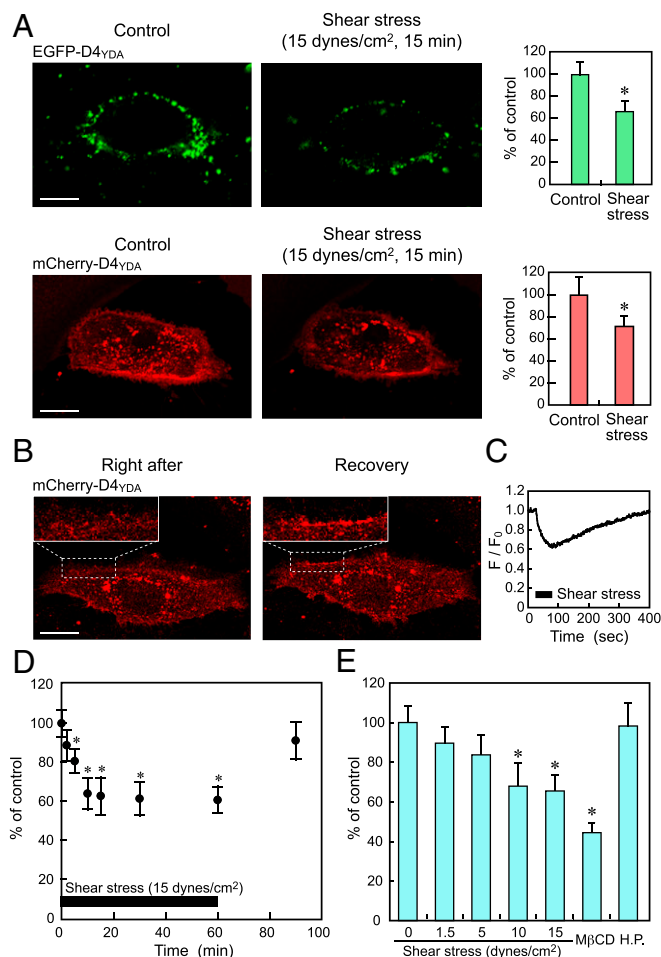
Fig. 2. Effects of shear stress on the cholesterol levels in EC plasma membranes. (*A*) Confocal images of HPAECs labeled with EGFP-D4$_{YDA}$ and expressing mCherry-D4$_{YDA}$ obtained before (Control) and 15 min after shear stress (15 dynes/cm^2) loading. The bar graphs in *Right* show the results of quantitative analyses. The data are expressed as the mean ± SD (*n* = 20). Shear stress markedly reduced both the EGFP-D4$_{YDA}$ and mCherry-D4$_{YDA}$ signals in the plasma membranes. A similar phenomenon was observed in many other cells subjected to shear stress. (Scale bars: 20 μm.) *P < 0.01 vs. control. (*B*) Confocal images of mCherry-D4$_{YDA}$ obtained before (Control), immediately after (Right after), and 5 min after (Recovery) shear stress loading. *Upper Left Insets* show enlarged images of the cell membrane surrounded by the broken line. The decreased cholesterol levels had returned to the control levels when examined 5 min after the cessation of the shear stress. (Scale bar: 20 μm.) (*C*) Shear stress-induced temporal changes in cholesterol in the inner bilayer in a representative cell. Real-time imaging of mCherry-D4$_{YDA}$ showed that inner plasma membrane cholesterol began to decease immediately after the initiation of the shear stress and that the decreased cholesterol levels recovered gradually after the shear stress was stopped. A similar phenomenon was observed in many other cells. All of the above experiments were performed with the cells in a non-confluent state. (*D*) Shear stress-induced temporal changes in cholesterol in the outer bilayer as quantified using flow cytometric analysis of cells labeled with EGFP-D4$_{YDA}$. The cholesterol levels rapidly and significantly decreased in response to shear stress, and the decreased cholesterol levels returned to the control level after the cessation of the shear stress. Values are the mean ± SD of nine samples obtained in three separate experiments. *P < 0.01 compared with static control. (*E*) Intensity dependency of shear stress-induced changes in cholesterol levels. HPAECs were exposed to shear stress at different intensities for 10 min, and changes in the cholesterol level were examined using flow cytometry. Cholesterol levels decreased further as the intensity of the shear stress increased until a value of 10 dynes/cm^2 was reached. Treatment of the cells with MβCD (10 mM) decreased the outer bilayer cholesterol levels to around 40% of the value in the control. Hydrostatic pressure (H.P.; 40 mm Hg) was applied to cells under no-flow

findings indicate that shear stress increased ATP production by enhancing mitochondrial oxidative phosphorylation, but not cytosolic glycolysis. Similar to shear stress loading, treatment of the cells with MβCD, which depletes membrane cholesterol, markedly increased the ATP levels in the mitochondria (Fig. 4*B*). This result indicated that a reduction in the plasma membrane cholesterol level alone can activate mitochondrial oxidative phosphorylation.

The addition of different concentrations of cholesterol to cells inhibited both the shear stress- and MβCD-induced increases in mitochondrial ATP production in a dose-dependent manner and almost abolished the effects of shear stress and MβCD at 100 μM cholesterol (Fig. 4 *C–F*). Flow cytometry analyses of ECs labeled with EGFP-D4$_{YDA}$ showed that the addition of cholesterol prevented the shear stress-induced decrease in plasma membrane cholesterol in a dose-dependent manner (*SI Appendix*, Fig. S3). These findings indicated that a reduction in the plasma membrane cholesterol is closely coupled to the increasing effect of shear stress on mitochondrial ATP production in ECs.

Discussion

The present study demonstrated that D4 imaging enabled the depiction of cholesterol in the plasma membranes of living cells. Both EGFP-D4$_{YDA}$ and mCherry-D4$_{YDA}$ signals were localized to the plasma membranes, but because of the limited resolution of the microscope, it was not possible to separate the cholesterol distributed in the outer and inner bilayers of the plasma membrane visually in the same cell. D4 imaging and flow cytometry showed that shear stress markedly decreased the plasma membrane cholesterol in HPAECs, which was consistent with the biochemical measurements of cholesterol. The decrease in the plasma membrane cholesterol level occurred rapidly mainly in the apical plasma membranes, and it was shear stress dependent and reversible. Although the mechanism by which shear stress decreases plasma membrane cholesterol levels remains unclear, it may be related to water entering the plasma membranes in a lipid order-dependent manner. Our previous studies using Laurdan fluorescence imaging revealed that the amount of water entering the lipid bilayer increased as the lipid order of the plasma membrane decreased in response to shear stress (8), thereby providing suitable conditions for hydrophobic cholesterol to leave the plasma membranes.

Until now, various probes, including Filipin (27), boron-dipyrromethene (BODIPY) cholesterol (28, 29), and Dehydroergosterol (30), have been used to analyze the dynamics of cellular cholesterol, but each of these probes has its own set of pros and cons (31, 32). In particular, many probes are not suitable for the analysis and imaging of living cells because their fluorescence is quenched too rapidly, their excitation wavelengths are cytotoxic, or their binding to cholesterol perturbs the cell membrane. The D4 of PFO binds to cholesterol with a high affinity (K_d ∼ 10^{-8}) but is not cytotoxic (33). Therefore, recombinant EGFP-D4 and mCherry-D4 proteins have been used to visualize cholesterol in mammalian cells. Recently, probes with mutations in D4 resulting in a higher affinity for cholesterol have been used (25). These probes are also suitable for quantifying alterations in the plasma membrane cholesterol content by subjecting the cells labeled with EGFP-D4 to flow cytometry. However, it should be noted that there is a threshold concentration of membrane cholesterol for D4 binding. D4 does not bind unless the amount of cholesterol in the plasma membrane exceeds 35 mol% of the total lipids, so cells with relatively low membrane cholesterol contents

conditions but had no effect on the cholesterol levels. Values are the mean ± SD of six samples obtained in two separate experiments. Experiments in *D* and *E* were performed with the cells in a confluent state. *P < 0.01 compared with a static control.
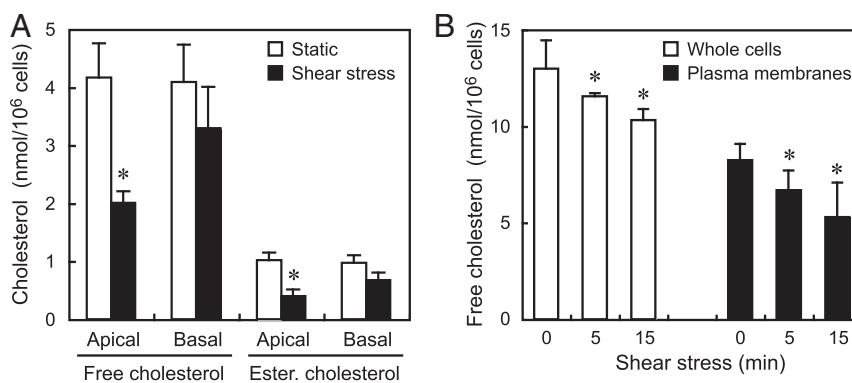
PHYSIOLOGY

Fig. 3. Effects of shear stress on the free and esterified cholesterol contents of the apical and basal plasma membranes and whole cells. HPAECs were subjected to a shear stress of 15 dynes/cm^2 for 15 min and were examined biochemically for changes in their cholesterol contents. (*A*) Changes in the free and esterified cholesterol contents of the apical and basal plasma membranes. Shear stress significantly decreased both the free and esterified cholesterol contents in the apical membranes, but not in the basal membranes. Values are the mean ± SD of nine samples obtained from three separate experiments. *$P < 0.01$ compared with a static control. (*B*) Changes in the free cholesterol contents of whole cells and isolated plasma membranes. Shear stress significantly decreased the cholesterol content of the whole cells as well as the plasma membranes, indicating that a certain amount of plasma membrane cholesterol moved out of the cells and the remainder moved into the cells. Values are the mean ± SD of nine samples obtained from three separate experiments. All of the above experiments were performed with the cells in a confluent state. *$P < 0.01$ compared with a static control (zero shear stress).

cannot be visualized. The use of EGFP-D4$_{YDA}$ and mCherry-D4$_{YDA}$ allowed us to visualize plasma membrane cholesterol and intracellular organelle cholesterol clearly in living HPAECs.

Biochemical analysis and real-time imaging of mCherry-D4$_{YDA}$ showed that shear stress caused both the efflux and the internalization of plasma membrane cholesterol in ECs, although the percentages of cholesterol moving in each of the two directions was not determined. Concerning cholesterol efflux, there are at least two independent mechanisms: the desorption of plasma membrane cholesterol into the aqueous phase followed by diffusion and cholesterol acceptor-mediated pathways (34). The cholesterol efflux that occurred under the present conditions was thought to have involved the former mechanism since the perfusate, Hank's balanced salt solution (HBSS), used in the flow-loading experiments did not contain any cholesterol acceptors, such as high-density lipoprotein, apolipoprotein, or bovine serum albumin. However, the means by which plasma membrane cholesterol is released into the aqueous phase is currently unclear. Since free cholesterol is known to have a limited but finite aqueous solubility in the 10-nM range, cholesterol itself can move into perfusates in response to shear stress. As other possibilities, cholesterol could be released as a molecular assembly combined with other components of the plasma membrane (e.g., phospholipids) or within vesicles. Regarding cholesterol internalization, several possible mechanisms may be involved, including aqueous diffusion; vesicle-mediated transport; and nonvesicular, carrier-mediated transport involving sterol transfer proteins (35). Further studies are needed to identify whether these mechanisms work separately or together to internalize plasma membrane cholesterol under shear stress.

As shown in our previous study, HPAECs immediately increase their mitochondrial ATP production in response to shear stress, which causes the release of ATP out of the cell and subsequent purinergic Ca^{2+} signaling (18). The present study has revealed the involvement of plasma membrane cholesterol dynamics in shear stress-induced mitochondrial ATP production. The addition of cholesterol to the cells inhibited both the decreasing effect of shear stress on the plasma membrane cholesterol level and its increasing effect on mitochondrial ATP production in a dose-dependent manner. Interestingly, the treatment of ECs with MβCD, which depletes plasma membrane cholesterol, alone resulted in an increase in mitochondrial ATP production, and the addition of cholesterol prevented the increasing effect of MβCD on ATP production. At present, however, it remains unclear how changes in the plasma membrane cholesterol levels influence mitochondrial

oxidative phosphorylation. Although no direct evidence is available, several possible mechanisms can be speculated. The first possibility is related to O$_2$ permeation. Since membrane cholesterol acts as a barrier to limit the permeation of O$_2$ into cells (36, 37), its reduction may increase the amount of O$_2$ reaching the mitochondria, thereby influencing the electron transfer chain reactions (38). Another possibility is related to the cholesterol content of mitochondrial membranes. The functions of mitochondria are closely coupled to changes in their membrane cholesterol levels (39). For instance, increased mitochondrial cholesterol levels impair mitochondrial oxidative phosphorylation by decreasing the mitochondrial membrane potential and fluidity and disrupting the assembly of respiratory supercomplexes (40), whereas decreased cholesterol levels in mitochondrial membranes increase ATP synthase activity (41). Thus, if a reduction in plasma membrane cholesterol leads to a decrease in mitochondria membrane cholesterol, ATP production might be augmented. A further possibility is the involvement of mechanosensitive receptors and ion channels. Since plasma membrane cholesterol dynamics are known to influence the activities of receptors and ion channels expressed on the plasma membrane (42), a reduction in plasma membrane cholesterol may activate mitochondrial oxidative phosphorylation via their downstream signaling pathways, such as through an increase in intracellular and mitochondrial Ca^{2+} concentrations (43, 44).

HPAECs have abundant caveolae, which are small flask-shaped invaginations of the plasma membrane, rich in cholesterol and sphingolipids. Caveolae possess caveolin, which is an essential protein for maintaining their structure; caveolin also functions as a scaffolding protein that interacts with many signaling molecules. Therefore, caveolae are known to play a role not only in endocytosis, transcytosis, and cholesterol homeostasis but also, in signal transduction (45). Many studies have revealed that caveolae are also involved in the mechanotransduction of shear stress. When bovine aortic ECs were subjected to shear stress, the phosphorylation of caveolin occurred immediately, mediating shear stress-induced integrin signaling and subsequent cytoskeletal rearrangement (46). We demonstrated that the application of shear stress to HPAECs caused an immediate release of ATP at the caveolae, from which Ca^{2+} waves were propagated throughout the cell (14). We also showed that shear stress rapidly caused a phase transition from a liquid-ordered phase to a liquid-disordered phase in the caveola-rich plasma membrane (8). The reduction in lipid order seen at caveola sites and the decrease in membrane cholesterol observed in the present study suggest that
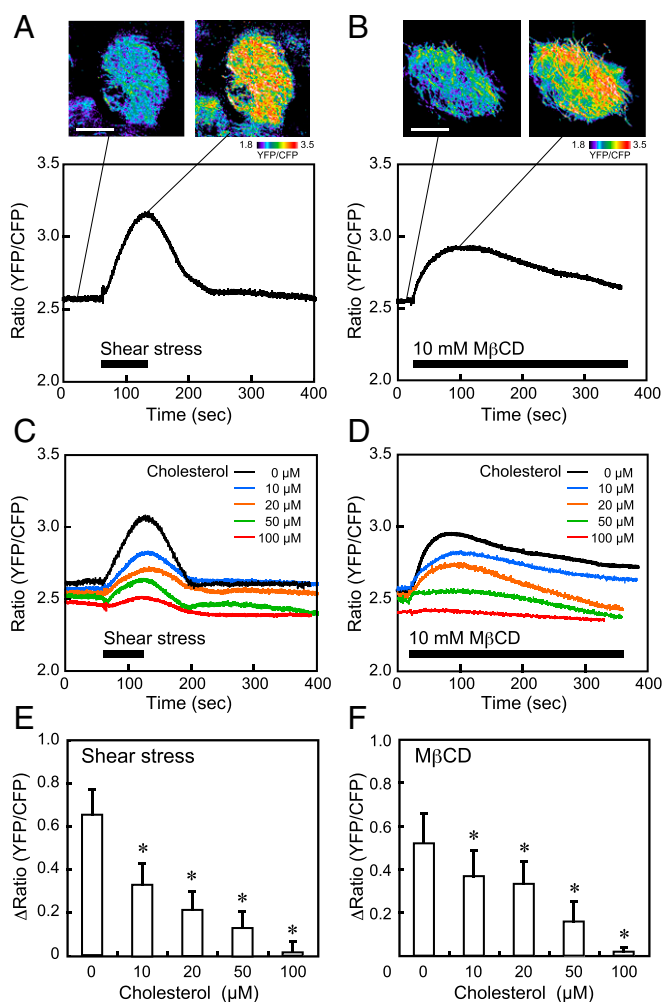
Fig. 4. Effects of shear stress and MβCD on mitochondrial ATP levels. HPAECs were subjected to a shear stress of 15 dynes/cm^2 and were examined for changes in the mitochondrial ATP level, which was determined using the FRET-based ATP biosensor mitAT1.03. (*A*) Typical example of shear stress-induced mitochondrial ATP production. Pseudocolor images of the YFP-to-CFP ratio showed that shear stress markedly increased the ATP levels in the mitochondria. The colors represent the ATP levels indicated by the scale. The time course of the YFP-to-CFP ratio showed that the ATP level rapidly increased in response to shear stress and then returned to the control level after the shear stress ceased. Similar mitochondrial reactions were also observed in many other cells in different experiments. (Scale bar: 20 μm.) (*B*) Typical example of MβCD-induced mitochondrial ATP production. The ATP levels increased rapidly in response to the treatment of cells with MβCD; after reaching the maximum level, the levels gradually declined. Similar reactions were also observed in many other cells. (Scale bar: 20 μm.) (*C* and *D*) Effects of cholesterol addition on the shear stress- and MβCD-induced increase in ATP production. Solutions with different concentrations of cholesterol (0, 10, 20, 50, and 100 μM), prepared with water-soluble cholesterol powder (Sigma-Aldrich C4951) in which cholesterol was incorporated into MβCD (molar ratio, 1:7), were added to the cells. An example of the mitochondrial ATP reaction at each concentration of cholesterol is shown. The addition of cholesterol to the cells inhibited the increasing effects of shear stress and MβCD on mitochondrial ATP production in a dose-dependent manner and almost abolished them at 100 μM cholesterol. (*E* and *F*) Quantitative analysis of the effects of cholesterol addition on mitochondrial ATP production. The bar graphs showed a dose-dependent inhibition of both shear stress- and MβCD-induced mitochondrial ATP production by the addition of cholesterol. Results are presented as the mean ± SD of 15 samples obtained in three separate experiments. All of the above experiments were performed with the cells in a confluent state. *$P < 0.01$ compared with the control (zero cholesterol).

shear stress reduces or dissolves caveolae. Emerging evidence suggests that caveolae and caveolin proteins modulate mitochondrial biogenesis, structure, and function (47). Mitochondria are also in close proximity to caveolae, and some structures exist between them (48). Therefore, it seems possible that shear stress affects mitochondrial functions by changing the dynamics of caveolae and caveolin. Such studies on caveola–mitochondrial coupling would provide a new perspective on the mechanism of shear stress mechanotransduction.

The present study showed that plasma membrane cholesterol dynamics play an important role in the HPAEC response to shear stress (i.e., the activation of mitochondrial oxidative phosphorylation). The involvement of membrane cholesterol in cellular mechanoresponses has also been shown in other types of cells, including bovine aortic ECs (22), osteoblasts (49), and leukocytes (50). Changes in plasma membrane cholesterol levels are thought to affect cell functions through a variety of pathways, including those via changes in membrane physical properties such as stiffness and fluidity, cholesterol-rich caveolae and rafts, cellular cholesterol metabolism, and the cholesterol content of intracellular organelle membranes. Membrane cholesterol also regulates the function of membrane receptors and ion channels by altering their conformation and assembly via changes in membrane physical properties and specific binding (51, 52). Many types of ion channels are known to be regulated by membrane cholesterol (19), and recently, the human mechanosensitive ion channel Piezo1, which is gated by membrane tension and also acts as a flow sensor in ECs, has been shown to be modified by membrane cholesterol (53); specifically, cholesterol enrichment or depletion by MβCD and the disruption of membrane cholesterol organization using the dynamin inhibitor dynasore changed the Piezo1 response to mechanical force. Thus, to elucidate the mechanism of EC mechanotransduction, clarifying the role of plasma membrane cholesterol dynamics in cell responses to biomechanical forces is essential. Solving this problem would lead to a better understanding of how hemodynamic forces influence circulatory homeostasis and the pathogenesis of vascular diseases, such as aneurysms and atherosclerosis.

Materials and Methods

Cell Cultures. HPAECs were purchased from Lonza Walkersville Inc. (product code: cc-2530) and were grown in medium 199 supplemented with 15% fetal bovine serum, 2 mM L-glutamine (Gibco), 50 μg/mL heparin, and 30 μg/mL EC growth factor (Becton Dickinson) in a 1% gelatin-coated tissue culture flask. The cells used in the experiments in this study were in the 7th and 10th passages. All of the experiments were approved by the Ethics Committee of the University of Tokyo, Graduate School of Medicine. Most experiments were performed with the cells in a confluent state, but some experiments were performed in a nonconfluent state to visualize plasma membrane cholesterol clearly.

Shear Stress Experiments. Cells were subjected to controlled levels of laminar shear stress in a parallel plate-type flow-loading device (FCS2; Bioptechs), as previously described (54). Briefly, the flow chamber consisted of a 1% gelatin-coated cover glass with the cultured cells on one side and a second parallel glass plate held 200 μm apart from the first plate by a Teflon gasket. The medium was perfused using a roller/tube pump, and the entire closed circuit was maintained at exactly 37 °C. The intensity of the shear stress (τ; dynes per centimeter squared) acting on the EC layer was calculated from the formula $τ = 6μQ/a^2b$, where μ is the viscosity of the perfusate (poise), Q is the flow volume (milliliters per second), and a and b are the cross-sectional dimensions of the flow path (centimeters).

Cholesterol Probes.
EGFP-D4$_{YDA}$ protein. A plasmid containing hexahistidine (6xHis) tag-fused *EGFP-D4* cloned with the pET28b vector was a gift from Toshihide Kobayashi, University of Strasbourg, Strasbourg, France. To increase the cholesterol affinity of the EGFP-D4 protein, three amino acids in the D4 were mutated (Y415A, D434W, and A463W), creating EGFP-D4$_{YDA}$ (25). *Escherichia coli* BL21 (DE3; Novagen) was transformed using the pET28b-EGFP-D4$_{YDA}$

plasmid and then cultured in Luria-Bertani broth (Formedium) containing 50 µg/mL kanamycin (Wako) at 37 °C until the optical density (OD_{600}) reached 0.4. Then, 1 mM isopropyl β-D-thiogalactopyranoside (Wako) was added to the medium, and the cultures were induced for 3 h at 37 °C; 6xHis-tagged EGFP-D4$_{YDA}$ protein was purified using Ni-NTA Agarose (QIAGEN) and concentrated using an ultrafiltration column (Amicon Ultra-15 10K; Merck Millipore), according to the manufacturers' instructions. The protein was analyzed using sodium dodecyl sulfate/polyacrylamide gel electrophoresis with 0.1% Coomassie brilliant blue staining and Western blotting with an anti-6xHis tag antibody (Abcam).

Adenovirus of mCherry-D4$_{YDA}$. D4$_{YDA}$ was introduced into a pFPV-mCherry vector at the *Hind*III/*Xho*I site. Complementary deoxyribonucleic acid (cDNA) of *mCherry-D4$_{YDA}$* was cloned into a pAd-CMV-V5-DEST Gateway vector (Thermo Fisher Scientific) using LR recombination reactions, and an adenovirus vector containing *mCherry-D4$_{YDA}$* cDNA (Ad-mCherry-D4$_{YDA}$) was constructed. The cultured HPAECs were infected with 50 plaque-forming units per cell of Ad-mCherry-D4$_{YDA}$.

Imaging of cholesterol, PLC, and TfR. PH-PLCD1-GFP, PH-PLCD1-iRFP, and TfR-GFP plasmids were purchased from Addgene (plasmids 51407, 66841, and 45060, respectively) and were transfected into cultured HPAECs using the Neon Transfection System (Thermo Fisher) 2 d before imaging under optimized conditions (1,270 V, 20-ms pulse length, with two pulses). All of the images were captured using a confocal laser-scanning microscope (A1R HD25; Nikon) equipped with ×60 (ApoTIRF) and ×100 (SR ApoTIRF) objectives at the following excitation/emission wavelengths: EGFP-D4, PH-PLCD1-GFP, and TfR-GFP (488, 525/50 nm); mCherry-D4 (561, 595/50 nm); and PH-PLCD1-iRFP (640, 700/75 nm) using NIS-Elements C software (Nikon). The obtained images were merged using Adobe Photoshop software. Signals of D4-based sensors were quantitatively analyzed by Image Pro-10 software (Media Cybernetics).

Flow cytometry. Cholesterol in the outer plasma membrane bilayer of HPAECs was labeled with the EGFP-D4$_{YDA}$ protein and measured using a Gallios flow cytometer (Beckman Coulter). A total of 1×10^6 cells were incubated with the EGFP-D4$_{YDA}$ protein (30 µg/mL) for 10 min on ice. The cells were rinsed with HBSS twice before analysis. The cell counts vs. logarithmic fluorescent intensity histograms were recorded for 2×10^5 cells for each sample. Background fluorescence was obtained using nonlabeled cells. The cholesterol contents were statistically analyzed using Kaluza Analysis Flow Cytometry Software, version 2.1.1 (Beckman Coulter).

Biochemical measurements of cholesterol. The amounts of cholesterol in whole cells and isolated plasma membranes were biochemically measured according to previously described methods (10). Plasma membranes were prepared as described previously (55). Briefly, cells were homogenized with a Teflon homogenizer (Wheaton) and centrifuged at $1,000 \times g$ for 10 min. The postnuclear supernatant was collected, and the plasma membrane fraction was isolated using 30% Percoll-gradient fractionation ($84,000 \times g$ for 30 min)

and extracted with chloroform/isopropyl alcohol/Nonidet P-40 (7:11:0.1). The apical and basal membranes were isolated from cultured HPAECs using cationic colloidal silica (Nalco 1060) and polyacrylic acid sodium salt (molecular weight ~ 5,100; Sigma-Aldrich), according to a previously reported procedure (56). Free cholesterol and cholesteryl ester (esterified cholesterol) in the apical and basal plasma membrane fractions were assayed spectrophotometrically using a cholesterol quantitation kit (BioVision Inc.) and a microplate reader (ARVO SX; Perkin-Elmer Life Sciences) according to the manufacturers' instructions and normalizing the value according to the protein concentration and cell number.

Imaging of mitochondrial ATP. The mitochondrial ATP was imaged using an FRET-based ATP biosensor targeted at the mitochondrial matrix (*mitAT1.03*), as previously described (26). The cDNA of *mitAT1.03* was ligated and cloned into the *Sal*I/*Not*I sites of a pAd-CMV-V5-DEST Gateway Vector (Thermo Fisher Scientific), and the adenovirus vector containing *mitAT1.03* cDNA (Ad-mitAT1.03) was constructed as described previously. Cultured HPAECs were infected with 50 plaque-forming units per cell of Ad-mitAT1.03.

Three to five days after Ad-mitAT1.03 infection, the HPAECs (maintained at 37 °C) were imaged using an ECLIPSE Ti-E inverted microscope (Nikon) with ×60 and ×100 ApoTIRF oil objectives (1.49 numerical aperture) using a water-cooling electron multiplier charge-coupled device camera (ImagEM C9100-13; Hamamatsu) controlled by HCImage software, version 4.3 (Hamamatsu). Dual-emission ratio imaging of mitAT1.03 was performed using an FF01-427/10 excitation filter (Semrock), an FF458-Di01 dichroic mirror, and a Dual View Multichannel Imaging System (DV2; Photometrics) equipped with two emission filters (FF01-483/32 for CFP and FF01-542/27 for YFP). The images were analyzed using MetaMorph software, version 7.7 (Molecular Devices).

Statistical analysis. The results are presented as the mean ± SD. Statistical significance was evaluated using an ANOVA with the Bonferroni adjustment applied to the results of post hoc *t* tests. The statistical analysis was performed using SPSS software (SPSS Inc.). A *P* value of <0.05 was regarded as being statistically significant.

Data Availability. All study data are included in the article and *SI Appendix*.

1. P. F. Davies, Flow-mediated endothelial mechanotransduction. *Physiol. Rev.* **75**, 519–560 (1995).
2. T. Aoki *et al.*, PGE(2) -EP(2) signalling in endothelium is activated by haemodynamic stress and induces cerebral aneurysm through an amplifying loop via NF-κB. *Br. J. Pharmacol.* **163**, 1237–1249 (2011).
3. J. J. Chiu, S. Chien, Effects of disturbed flow on vascular endothelium: Pathophysiological basis and clinical perspectives. *Physiol. Rev.* **91**, 327–387 (2011).
4. K. Yamamoto *et al.*, Impaired flow-dependent control of vascular tone and remodeling in P2X4-deficient mice. *Nat. Med.* **12**, 133–137 (2006).
5. Y. Fang, D. Wu, K. G. Birukov, Mechanosensing and mechanoregulation of endothelial cell functions. *Compr. Physiol.* **9**, 873–904 (2019).
6. P. J. Butler, G. Norwich, S. Weinbaum, S. Chien, Shear stress induces a time- and position-dependent increase in endothelial cell membrane fluidity. *Am. J. Physiol. Cell Physiol.* **280**, C962–C969 (2001).
7. T. Tabouillot, H. S. Muddana, P. J. Butler, Endothelial cell membrane sensitivity to shear stress is lipid domain dependent. *Cell. Mol. Bioeng.* **4**, 169–181 (2011).
8. K. Yamamoto, J. Ando, Endothelial cell and model membranes respond to shear stress by rapidly decreasing the order of their lipid phases. *J. Cell Sci.* **126**, 1227–1234 (2013).
9. P. J. Butler, T. C. Tsou, J. Y. Li, S. Usami, S. Chien, Rate sensitivity of shear-induced changes in the lateral diffusion of endothelial cell membrane lipids: A role for membrane perturbation in shear-induced MAPK activation. *FASEB J.* **16**, 216–218 (2002).
10. K. Yamamoto, J. Ando, Vascular endothelial cell membranes differentiate between stretch and shear stress through transitions in their lipid phases. *Am. J. Physiol. Heart Circ. Physiol.* **309**, H1178–H1185 (2015).
11. K. Yamamoto, J. Ando, Emerging role of plasma membranes in vascular endothelial mechanosensing. *Circ. J.* **82**, 2691–2698 (2018).
12. J. Ando, K. Yamamoto, Flow detection and calcium signalling in vascular endothelial cells. *Cardiovasc. Res.* **99**, 260–268 (2013).
13. P. Bodin, D. Bailey, G. Burnstock, Increased flow-induced ATP release from isolated vascular endothelial cells but not smooth muscle cells. *Br. J. Pharmacol.* **103**, 1203–1205 (1991).
14. K. Yamamoto *et al.*, Visualization of flow-induced ATP release and triggering of Ca²⁺ waves at caveolae in vascular endothelial cells. *J. Cell Sci.* **124**, 3477–3483 (2011).
15. S. Wang *et al.*, P2Y₂ and Gq/G₁₁ control blood pressure by mediating endothelial mechanotransduction. *J. Clin. Invest.* **125**, 3077–3086 (2015).
16. K. Yamamoto, R. Korenaga, A. Kamiya, J. Ando, Fluid shear stress activates Ca²⁺ influx into human endothelial cells via P2X4 purinoceptors. *Circ. Res.* **87**, 385–391 (2000).
17. K. Yamamoto *et al.*, P2X(4) receptors mediate ATP-induced calcium influx in human vascular endothelial cells. *Am. J. Physiol. Heart Circ. Physiol.* **279**, H285–H292 (2000).
18. K. Yamamoto, H. Imamura, J. Ando, Shear stress augments mitochondrial ATP generation that triggers ATP release and Ca²⁺ signaling in vascular endothelial cells. *Am. J. Physiol. Heart Circ. Physiol.* **315**, H1477–H1485 (2018).
19. I. Levitan, Y. Fang, A. Rosenhouse-Dantsker, V. Romanenko, Cholesterol and ion channels. *Subcell. Biochem.* **51**, 509–549 (2010).
20. Z. Hong, M. C. Staiculescu, P. Hampel, I. Levitan, G. Forgacs, How cholesterol regulates endothelial biomechanics. *Front. Physiol.* **3**, 426 (2012).
21. Y. Fu *et al.*, A novel mechanism of γ/δ T-lymphocyte and endothelial activation by shear stress: The role of ecto-ATP synthase β chain. *Circ. Res.* **108**, 410–417 (2011).
22. H. Park *et al.*, Plasma membrane cholesterol is a key molecule in shear stress-dependent activation of extracellular signal-regulated kinase. *J. Biol. Chem.* **273**, 32304–32311 (1998).
23. X. Sun *et al.*, Activation of integrin α5 mediated by flow requires its translocation to membrane lipid rafts in vascular endothelial cells. *Proc. Natl. Acad. Sci. U.S.A.* **113**, 769–774 (2016).
24. M. Maekawa, Domain 4 (D4) of perfringolysin O to visualize cholesterol in cellular membranes-the update. *Sensors (Basel)* **17**, 504 (2017).
25. S. L. Liu *et al.*, Orthogonal lipid sensors identify transbilayer asymmetry of plasma membrane cholesterol. *Nat. Chem. Biol.* **13**, 268–274 (2017).

26. H. Imamura *et al.*, Visualization of ATP levels inside single living cells with fluorescence resonance energy transfer-based genetically encoded indicators. *Proc. Natl. Acad. Sci. U.S.A.* **106**, 15651–15656 (2009).

27. H. Börnig, G. Geyer, Staining of cholesterol with the fluorescent antibiotic "filipin." *Acta Histochem.* **50**, 110–115 (1974).

28. M. Hölttä-Vuori *et al.*, BODIPY-cholesterol: A new tool to visualize sterol trafficking in living cells and organisms. *Traffic* **9**, 1839–1849 (2008).

29. Z. Li, E. Mintzer, R. Bittman, First synthesis of free cholesterol-BODIPY conjugates. *J. Org. Chem.* **71**, 1718–1721 (2006).

30. M. Mondal, B. Mesmin, S. Mukherjee, F. R. Maxfield, Sterols are mainly in the cytoplasmic leaflet of the plasma membrane and the endocytic recycling compartment in CHO cells. *Mol. Biol. Cell* **20**, 581–588 (2009).

31. M. Maekawa, G. D. Fairn, Molecular probes to visualize the location, organization and dynamics of lipids. *J. Cell Sci.* **127**, 4801–4812 (2014).

32. D. Wüstner, M. Modzel, F. W. Lund, M. A. Lomholt, Imaging approaches for analysis of cholesterol distribution and dynamics in the plasma membrane. *Chem. Phys. Lipids* **199**, 106–135 (2016).

33. Y. Shimada, M. Maruya, S. Iwashita, Y. Ohno-Iwashita, The C-terminal domain of perfringolysin O is an essential cholesterol-binding unit targeting to cholesterol-rich microdomains. *Eur. J. Biochem.* **269**, 6195–6203 (2002).

34. L. Liscum, N. J. Munn, Intracellular cholesterol transport. *Biochim. Biophys. Acta* **1438**, 19–37 (1999).

35. E. Ikonen, Cellular cholesterol trafficking and compartmentalization. *Nat. Rev. Mol. Cell Biol.* **9**, 125–138 (2008).

36. D. Dumas, V. Latger, M. L. Viriot, W. Blondel, J. F. Stoltz, Membrane fluidity and oxygen diffusion in cholesterol-enriched endothelial cells. *Clin. Hemorheol. Microcirc.* **21**, 255–261 (1999).

37. N. Khan *et al.*, Plasma membrane cholesterol: A possible barrier to intracellular oxygen in normal and mutant CHO cells defective in cholesterol metabolism. *Biochemistry* **42**, 23–29 (2003).

38. E. Gnaiger, R. Steinlechner-Maran, G. Méndez, T. Eberl, R. Margreiter, Control of mitochondrial and cellular respiration by oxygen. *J. Bioenerg. Biomembr.* **27**, 583–596 (1995).

39. M. Bosch *et al.*, Caveolin-1 deficiency causes cholesterol-dependent mitochondrial dysfunction and apoptotic susceptibility. *Curr. Biol.* **21**, 681–686 (2011).

40. E. Solsona-Vilarrasa *et al.*, Cholesterol enrichment in liver mitochondria impairs oxidative phosphorylation and disrupts the assembly of respiratory supercomplexes. *Redox Biol.* **24**, 101214 (2019).

41. W. Yu *et al.*, Altered cholesterol metabolism in Niemann-Pick type C1 mouse brains affects mitochondrial function. *J. Biol. Chem.* **280**, 11731–11739 (2005).

42. R. Phillips, T. Ursell, P. Wiggins, P. Sens, Emerging roles for lipids in shaping membrane-protein function. *Nature* **459**, 379–385 (2009).

43. B. R. Alevriadou, S. Shanmughapriya, A. Patel, P. B. Stathopulos, M. Madesh, Mitochondrial Ca^{2+} transport in the endothelium: Regulation by ions, redox signalling and mechanical forces. *J. R. Soc. Interface* **14**, (2017).

44. C. G. Scheitlin *et al.*, Endothelial mitochondria regulate the intracellular Ca^{2+} response to fluid shear stress. *Am. J. Physiol. Cell Physiol.* **310**, C479–C490 (2016).

45. P. W. Shaul, R. G. Anderson, Role of plasmalemmal caveolae in signal transduction. *Am. J. Physiol.* **275**, L843–L851 (1998).

46. C. Radel, V. Rizzo, Integrin mechanotransduction stimulates caveolin-1 phosphorylation and recruitment of Csk to mediate actin reorganization. *Am. J. Physiol. Heart Circ. Physiol.* **288**, H936–H945 (2005).

47. C. R. Foster, S. Satomi, Y. Kato, H. H. Patel, The caveolar-mitochondrial interface: Regulation of cellular metabolism in physiology and pathophysiology. *Biochem. Soc. Trans.* **48**, 165–177 (2020).

48. H. N. Fridolfsson *et al.*, Mitochondria-localized caveolin in adaptation to cellular stress and injury. *FASEB J.* **26**, 4637–4649 (2012).

49. J. T. Ferraro, M. Daneshmand, R. Bizios, V. Rizzo, Depletion of plasma membrane cholesterol dampens hydrostatic pressure and shear stress-induced mechanotransduction pathways in osteoblast cultures. *Am. J. Physiol. Cell Physiol.* **286**, C831–C839 (2004).

50. X. Zhang *et al.*, Membrane cholesterol modulates the fluid shear stress response of polymorphonuclear leukocytes via its effects on membrane fluidity. *Am. J. Physiol. Cell Physiol.* **301**, C451–C460 (2011).

51. M. A. Hanson *et al.*, A specific cholesterol binding site is established by the 2.8 A structure of the human β2-adrenergic receptor. *Structure* **16**, 897–905 (2008).

52. M. Zocher, C. Zhang, S. G. Rasmussen, B. K. Kobilka, D. J. Müller, Cholesterol increases kinetic, energetic, and mechanical stability of the human β2-adrenergic receptor. *Proc. Natl. Acad. Sci. U.S.A.* **109**, E3463–E3472 (2012).

53. P. Ridone, M. Vassalli, B. Martinac, Piezo1 mechanosensitive channels: What are they and why are they important. *Biophys. Rev.* **11**, 795–805 (2019).

54. K. Yamamoto *et al.*, Endogenously released ATP mediates shear stress-induced Ca^{2+} influx into pulmonary artery endothelial cells. *Am. J. Physiol. Heart Circ. Physiol.* **285**, H793–H803 (2003).

55. K. Yamamoto *et al.*, Involvement of cell surface ATP synthase in flow-induced ATP release by vascular endothelial cells. *Am. J. Physiol. Heart Circ. Physiol.* **293**, H1646–H1653 (2007).

56. D. B. Stolz, B. S. Jacobson, Examination of transcellular membrane protein polarity of bovine aortic endothelial cells in vitro using the cationic colloidal silica microbead membrane-isolation procedure. *J. Cell Sci.* **103**, 39–51 (1992).

PHYSIOLOGY